Propagation in a Waveguide Partially Filled with Anisotropic Dielectric Material

JAN I. H. ASKNE, MEMBER, IEEE, ERIK L. KOLLBERG, AND LARS PETTERSSON, MEMBER, IEEE

Abstract—**A rectangular waveguide partially filled with an anisotropic dielectric material has been studied. The method of analysis has been shown to be quite powerful. A new configuration with a rectangular waveguide unsymmetrically loaded with a rectangular dielectric insert has been analyzed and tested experimentally. The special effects of mode coupling by breaking the symmetry of the structure are studied and the consequences for single-mode operation with application to masers in the millimeter-wave region are demonstrated.**

I. Introduction

DURING RECENT years considerable interest has been focused on dielectric waveguides. The development of theories and numerical methods has been stimulated by the potential use of dielectric waveguides for integrated circuits in the millimeter-wave frequency region up to optical frequencies.

In this paper we will discuss and analyze wave propagation in rectangular waveguides loaded with a rectangular dielectric insert of high dielectric constant (Fig. 1). The present interest in this problem arose in connection with the realization of maser amplifiers for the frequency range 20–40 GHz [1]. The maser crystal (iron-doped TiO_2), which in the present design study is identical with the dielectric loading in Fig. 1, has a very high and anisotropic dielectric constant, ϵ_r is 170 along the x-axis and 85 along the y- and z-axes. The image line (Fig. 1(b)) has earlier been studied in, for example [1], and the symmetrically loaded waveguide (Fig. 1(d)) has been studied in [2] and [3]. In the present paper we will consider changes in the dispersion relation when we gradually change the configuration from one to the other (Fig. 1(c)).

II. Method of Analysis

For dielectrically loaded waveguides of the type shown in Fig. 1, the field patterns of the modes of propagation cannot be described using analytical expressions in closed form. However, there are several algorithms available for solving eigenvalue and deterministic problems, which may be applied to more general types of waveguides such as the one treated in this paper. It is, however, by no means obvious which method is the most suitable when the dielectric insert of the waveguides in Fig. 1 has a large dielectric constant.

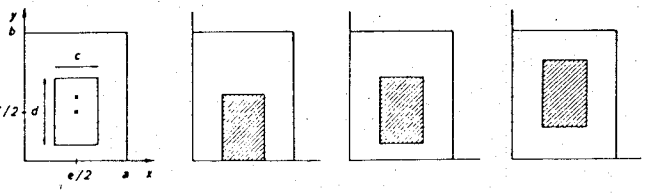

Fig. 1. Illustrating waveguides with dielectric insert. (a) Cross-sectional parameters. (b) Image line. (c) Unsymmetrically loaded. (d) Symmetrically loaded.

The method used by Lewin *et al.* [3] is accurate both for evaluation of the ω-k diagram and the field configuration. It is a mode-matching method similar to the least squares residual boundary method proposed by Davies [4], and requires some iteration procedure to find the minimum of the least square residual of the tangential field difference at the boundaries which may be rather costly. Schlosser and Unger [5] used a variational method, also fairly elaborate mathematically, which is somewhat limited concerning its accuracy since only two terms in the series expansion are used. Laloux *et al.* [2] expressed the differential equations by discretization. They used a variation-iteration method to solve the eigenvalue equations and applied the method on a waveguide loaded by an isotropic and lossy dielectric insert.

In this paper we will use an analysis which is based on the Galerkin method for analyzing nonideal waveguides discussed by Schelkunoff [6] and Johnson [7]. It can be shown that the final formulas are almost identical to those obtained from the method described by Ogusu [8]. The method yields a quite accurate ω-k diagram (the field pattern obtained is less accurate) with a moderate number of terms in the field expansions. This is so because the series are integrated, a procedure known to improve the convergence of slowly convergent series. The method is also mathematically fairly simple, as far as computing time is concerned and can easily be adopted to cases where the dielectric insert is anisotropic and offset from the center of the waveguide.

Since the method is rather closely related to the methods discussed in [6]–[8] for the isotropic case, we will here only point out the more essential steps in the derivation of the final formulas. The actual field is expanded in terms of the normalized and orthogonal field- or basis-functions $\bar{E}_n$ and

Manuscript received September 15, 1981; revised December 28, 1981. This work was supported by the Swedish Board for Technical Development.

J. I. H. Askne and E. L. Kollberg are with the Research Laboratory of Electronics, Chalmers University of Technology, S-412 96 Goteborg, Sweden.

L. Pettersson is with the National Defense Research Institute, Box 1165, S-581 11 Linkoping, Sweden.

0018-9480/82/0500-0795$00.75 ©1982 IEEE

$\bar{H}_n$. These functions have the same dependence on the transverse coordinates x and y as the normal modes of an empty waveguide, i.e., in this case the TE- and TM-modes of an empty rectangular waveguide. Hence

$$\bar{E}(x, y, z) = \sum_n \left[v_n(z)\bar{E}_{tn}(x, y) + q_n(z)\bar{E}_{zn}(x, y) \right] \tag{1}$$

$$\bar{H}(x, y, z) = \sum_n \left[i_n(z)\bar{H}_{tn}(x, y) + p_n(z)\bar{H}_{zn}(x, y) \right]. \tag{2}$$

Here $\bar{E}_{tn}$, $\bar{H}_{tn}$ and $\bar{E}_{zn}$, $\bar{H}_{zn}$ denote the transverse and longitudinal part of $\bar{E}_n$ and $\bar{H}_n$, respectively. The pertubation of the empty waveguide caused by the dielectric insert is taken into account by the expansion coefficients v_n, q_n, i_n, and p_n. These coefficients can be related to the real fields $\bar{E}$ and $\bar{H}$ by using the orthogonality properties. Since we have an inhomogeneous waveguide cross section, it is convenient to express the Maxwell equation as

$$\nabla \times \bar{H} = j\omega\epsilon_0 \bar{E} + j\omega\epsilon_0(\tilde{\epsilon}_r - 1)\bar{E} \tag{3}$$

where $\tilde{\epsilon}_r$ is the anisotropic dielectric constant matrix, being diagonal in our case. Using Maxwell's equations and the two dimensional Green's theorem we obtain, assuming perfectly conductive metal walls

$$p_n = v_n, \qquad \text{TE} \tag{4}$$

$$i_n = q_n + \frac{\epsilon_0 k_0^2}{\mu_0 \gamma_n^2} \int_S \bar{E}_{zn}^* \cdot (\tilde{\epsilon}_r - 1) \cdot \bar{E}\, dS, \qquad \text{TM} \tag{5}$$

$$\frac{\partial i_n}{\partial z} = -j\omega\epsilon_0 \left(v_n - \frac{\gamma_n^2}{k_0^2} \begin{Bmatrix} p_n \\ 0 \end{Bmatrix} + \int_S \bar{E}_{tn} \cdot (\tilde{\epsilon}_r - 1) \cdot \bar{E}\, dS \right), \quad \begin{Bmatrix} \text{TE} \\ \text{TM} \end{Bmatrix} \tag{6}$$

$$\frac{\partial v_n}{\partial z} = -j\omega\mu_0 \left(i_n - \frac{\gamma_n^2}{k_0^2} \begin{Bmatrix} 0 \\ q_n \end{Bmatrix} \right), \qquad \begin{Bmatrix} \text{TE} \\ \text{TM} \end{Bmatrix}. \tag{7}$$

The expressions are different if the basis function, denoted n, is a TE- or a TM-mode. γ_n is the transverse wavenumber for mode n. For the rectangular waveguide in Fig. 1, we have

$$\gamma_n^2 = \left(i\frac{\pi}{a} \right)^2 + \left(j\frac{\pi}{b} \right)^2 \tag{8}$$

where i and j are the integers associated with basis function n. Furthermore, we have $k_0^2 = \omega^2\epsilon_0\mu_0$ and S denotes the cross-sectional area of the dielectric insert. In fact, the integral over the dielectric insert represents the coupling between the modes of the empty waveguide. Assuming a z-dependence of $e^{-jk_z z}$ and inserting (1) and (2) into (4)–(7) yield equations linear in v_n, q_n, i_n, and p_n. We get the following matrix equations:

$$[p] = [v], \qquad \text{TE} \tag{9}$$

$$[i] = \tilde{X}[q], \qquad \text{TM} \tag{10}$$

$$k_z[i] = \tilde{Y}[v] \tag{11}$$

$$k_z[v] = \tilde{Z}[i] \tag{12}$$

where $[v]$, $[q]$, $[i]$, and $[p]$ are vectors of v_n, q_n, i_n, and p_n, $\tilde{X}$, $\tilde{Y}$, and $\tilde{Z}$ matrix with the following elements:

$$X_{nm} = \delta_{nm} + \frac{k_0^2}{Z_0^2 \gamma_n^2} \int_S \tilde{E}_{zn}^* \cdot (\tilde{\epsilon}_r(x, y) - 1)\bar{E}_{zm}\, dS, \qquad \text{TM} \tag{13}$$

$$Y_{nm} = \omega\epsilon_0 \left[\delta_{nm} \left(1 - \frac{\gamma_n^2}{k_0^2} \begin{Bmatrix} 1 \\ 0 \end{Bmatrix} \right) + \int_S \bar{E}_{tn}^* \cdot (\tilde{\epsilon}_r(x, y) - 1) \cdot \bar{E}_{tm}\, dS \right], \quad \begin{Bmatrix} \text{TE} \\ \text{TM} \end{Bmatrix} \tag{14}$$

$$Z_{nm} = \omega\mu_0 \left[\delta_{nm} - \begin{Bmatrix} 0 \\ \frac{\gamma_n^2}{k_0^2} (\tilde{X}^{-1})_{nm} \end{Bmatrix} \right], \quad \begin{Bmatrix} \text{TE} \\ \text{TM} \end{Bmatrix}. \tag{15}$$

The integrations are performed over the cross section. E_{tn}, etc. are the fields of the empty waveguide, and $\tilde{\epsilon}_r(x, y)$ is the (diagonal) dielectric constant tensor. With a rectangular rod in a rectangular waveguide the integrals can be determined analytically.

From (11) and (12) we obtain the eigenvalue equation

$$\tilde{Z}\tilde{Y}[v] = k_z^2[v]. \tag{16}$$

From (14)–(16) k_z^2 and v_n can be determined. The coefficients v_n, q_n, i_n, and p_n can be determined from the (9)–(12) for the TE- and TM-modes.

III. Numerical Analysis

We have tested our method by comparing with the exact method [9] for the *lowest* LSE-mode in a dielectric slab loaded waveguide in the same way as the variation-iteration method [10] was tested. We obtain perfect agreement. We *also* tested higher order LSE- and LSM-modes by comparing with the exact method. We conclude that for the three lowest order modes we obtained perfect agreement, while for the next four modes there was a difference in $\Delta f/f$ equal to 1, 1, 4, and 6 percent ($a = 1$, $b = 0.1$, $c = 0.25$, $d = 0.1$, $e = 1$, $f = 0.1$, $\epsilon_r = 16$, 2×12^2 modes were used, i.e., m and n varies between 0 and 11 for $\text{TE}_{m,n}$ and between 1 and 12 for $\text{TM}_{m,n}$ modes).

The dielectric image line was treated with a least-square-residual mode matching method in [3] and compared with the Rayleigh–Ritz variational method used in [5]. The same geometry was used to test the present mode coupling method with 2×10^2 modes (see Fig. 2). The agreement is quite good between the methods and the experimental results given in [5].

For dielectric rod waveguides, Fig. 1(d), Laloux *et al.* [2] and Lewin *et al.* [3] have presented numerical results for two different configurations. The corresponding results from our method do not agree particularly well with [2]. For the lowest mode the difference $\Delta f/f$ is 18 percent while the higher modes agree somewhat better. The results in [3] agree quite well with results from the present method.

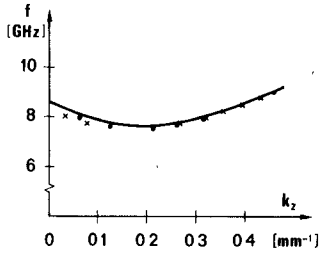

Fig. 2. Comparison between dispersion relation calculated with different methods: ——Schlosser–Unger [5]; · · · Lewin [4]; and xxx this paper. $a = 10.16$, $b = 6.00$, $c = 5.00$, $d = 4.00$, $e = 10.16$, and $f = 4.00$ mm. $\epsilon_r = 15$.

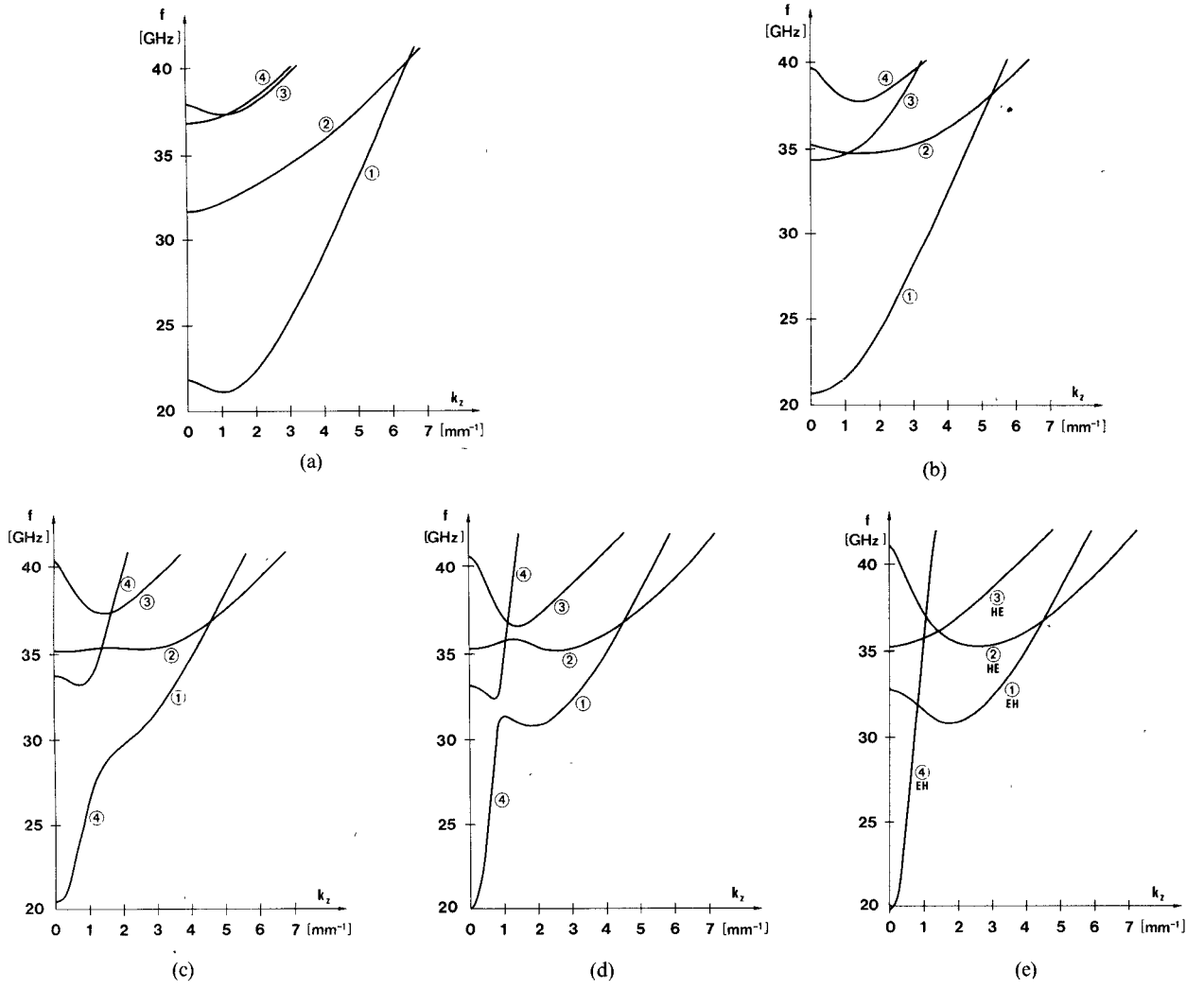

Fig. 3. Dispersion diagrams (frequency as function of propagation constant). $\epsilon_{rx} = 170$, $\epsilon_{ry} = \epsilon_{rz} = 85$. $a = 1.30$, $b = 1.60$, $c = 0.55$, $d = 0.82$, and $e = 1.30$ mm. (a) $f = 0.82$ mm (b) $f = 1.00$ mm (c) $f = 1.20$ mm (d) $f = 1.40$ mm (e) $f = 1.60$ mm.

Fig. 3 demonstrates results of computer calculations on a typical configuration with rutile ($\epsilon_{rx} = 170$, $\epsilon_{ry} = \epsilon_{rz} = 85$), using 2×10^2 modes. Tests have shown that increasing the number of modes further yields only a negligible change in the result for the dominating mode.

In order to discuss the changes in the dispersion diagram and the coupling between various modes, it is useful to first discuss the modes of the symmetrical case when $e = a$ and $f = b$. The symmetry group of the structure is then C_{2v} [12], and there are four nondegenerate mode classes corresponding to cases when the $(x, (b/2), z)$ plane and $((a/2), y, z)$ plane are either electric (conductive) walls ($E_{\tan} = 0$) or magnetic walls ($B_{\tan} = 0$). The four modes are classified as shown in Table I, where suffix o and e denotes the symmetry of the E_x-field versus $x = a/2$. The classification follows the nomenclature of Schlosser–Unger [5], and the field configurations of the four lowest order modes are illustrated in Fig. 4.

The asymptotic behavior of modes 1 and 2 is $k_z/\omega \cdot c_0 \approx \sqrt{\epsilon_y}$ and $\sqrt{\epsilon_x}$, respectively. The $_o$EH-mode, which has a

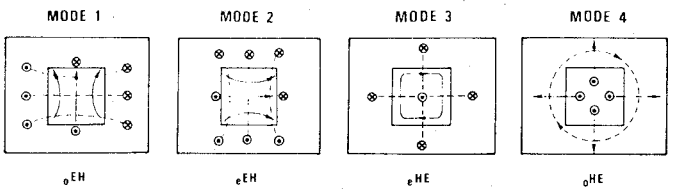

Fig. 4. Field configuration of the four lowest order fields. *E*-field is marked by solid lines, *H*-field by broken lines.

TABLE I
TABLE OVER VANISHING FIELD COMPONENTS FOR THE DIFFERENT MODES IN THE SYMMETRY PLANES

plane \ modes	1; $_0$EH	2; $_e$EH	3; $_e$HE	4; $_0$HE
$(x,\frac{b}{2},z)$	$E_x\ H_y\ E_z$	$H_x\ E_y\ H_z$	$E_x\ H_y\ E_z$	$H_x\ E_y\ H_z$
$(\frac{a}{2},y,z)$	$E_x\ H_y\ H_z$	$H_x\ E_y\ E_z$	$H_x\ E_y\ E_z$	$E_x\ H_y\ H_z$

backward wave region is the mode of interest in the maser application, where a low group velocity and a large concentration of the RF magnetic field to the inside of the crystal is wanted. For the $_o$EH-mode, these desired properties are particularly valid for such k-values where only one forward wave can exist. In the same frequency region another mode also exists which partially resembles the TEM-mode of a coaxial line, the $_o$HE-mode. Small irregularities in the structure will cause energy transfer (coupling) between these two modes. In a maser amplifier where an isolator is used for avoiding oscillations, this will cause problems since the $_o$HE-mode only weakly interacts with the isolator. Consequently, for the symmetric case we may in practice obtain unwanted oscillations in the maser amplifier. On the other hand, we can use the fact that these two modes have the same symmetry in the x-direction. By displacing the crystal in the y-direction the modes with the same symmetry in the x-direction will couple strongly to each other when their phase velocities are the same. According to Fig. 3, this happens in an area where one of the modes has a backward wave region. Then the coupled modes have energy flow in opposite directions while the stored energy is positive. This means (see e.g., [11]) that the coupling will result in a region with a complex propagation constant k and thus neither the unwanted part of the $_o$EH-mode nor the $_o$HE-mode will propagate. Computer results demonstrate this effect nicely. Fig. 3(d) shows the case of weak coupling and in Fig. 3(c) and (b) the coupling gets stronger. In Fig. 3(a) we have the image line case. The symmetry of this structure is C_{1v} [12], and there are now two nondegenerate mode classes. We conclude that the structure with the largest single-mode bandwidth is the structure illustrated in Fig. 3(b). With a high dielectric constant value the electric fields predominantly penetrate the dielectric surface perpendicularly and there is a strong discontinuity in the electric field. If also the distance between the waveguide wall and the dielectric insert becomes small, it is realized that a large number of the chosen basis functions become necessary to describe the fields accurately.

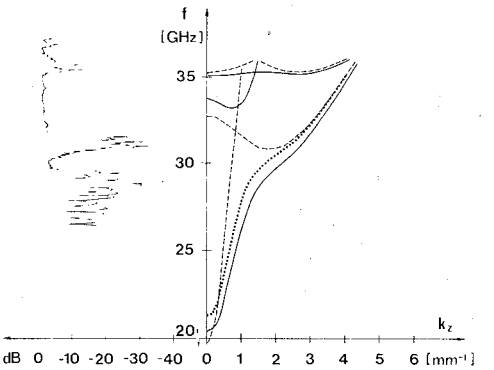

Fig. 5. Experimental results demonstrating insertion loss (left-hand part) and corresponding experimental dispersion diagram (· · ·) of structure (right-hand part). Numerical results from Fig. 3(c) marked by —— and Fig. 3(e) marked by ---- are included in right-hand part of figure.

We may conclude that the present method using 2×10^2 modes yields at least as accurate results as the methods mentioned above [3], [5]. Moreover, the present method is quite handy for analyzing more complicated (e.g., nonsymmetric) cross sections, and the computational costs are relatively low. The computation time on the central unit of an IBM 3033 N (4 MIPS) is 15 s for 2×10^2 modes and 40 s for 2×12^2 for the cases in Fig. 3.

IV. Experimental Results

Experimental dispersion diagrams have been obtained for some structures. A rutile crystal with the dimensions $c=0.55$ mm, $d=0.82$ mm, and a length of 67 mm was used in a waveguide $a=1.30$ mm and $b=1.60$ mm. The smallest value for f, 0.88 mm, was obtained with a 0.03-mm-thick sheet of teflon ($\epsilon_r=2$) between the waveguide wall and the crystal. The transmitted signal was attenuated according to the left-hand part of Fig. 5. The interference between the forward and reflected waves due to the length of the crystal was used to determine the dispersion diagram, as a dotted curve in the right-hand part of Fig. 5. Included in the dispersion diagram are the numerical results obtained with 2×10^2 modes calculated for $f=1.2$ mm when the teflon sheet is neglected. We obtain excellent agreement between the numerical analysis and the dispersion diagrams for high frequencies while for low frequencies, when the field is no longer concentrated inside the crystal, there is agreement only in the overall variation. In this region it is particularly important that the number of modes used in the computations is increased. However, taking into account the high value of the dielectric constant and the omission of the sheet of teflon in the calculation, the computational method is quite good.

V. Summary and Conclusion

By displacing a crystal inserted in a rectangular waveguide from the symmetrical position we have obtained a structure with interesting wave propagation properties such as a backward wave mode, as well as a region with complex propagation constant. With this type of structure one can avoid the problem of oscillations in a maser amplifier associated with the interaction between the backward wave

and the coaxial type of wave in the symmetrical case. We have, furthermore, obtained a single-mode structure with a high slowing factor and a low insertion loss compared to the image line structure where the crystal has to be soldered to the waveguide wall. The structure has been used successfully for a maser amplifier at 30 GHz [13], and the possibility to avoid oscillation problems may be of great value for construction of masers at even higher frequencies [14].

ACKNOWLEDGMENT

We would like to thank Å. Ljungbert for writing part of the computer program. We are also indebted to S. Galt for performing a lot of the experiments.

REFERENCES

[1] E. L. Kollberg and P. T. Lewin, "Traveling-wave masers for radio astronomy in the frequency range 20–40 GHz," *IEEE Trans. Microwave Theory Tech.*, vol. MTT-24, pp. 718–725, Nov. 1976.

[2] A. A. Laloux, R. J. M. Govaerts, and A. S. Vander Vorst, "Application of a variation-iteration method to waveguides with inhomogeneous lossy loads," *IEEE Trans. Microwave Theory Tech.*, vol. MTT-22, pp. 229–236, Mar. 1979.

[3] T. Lewin, J. Järnmark, and E. Kollberg, "Theoretical and experimental evaluation of high permittivity dielectric rod waveguides," *Int. J. Electron*, vol. 49, pp. 147–159, no. 2, 1980.

[4] J. B. Davies, "A least-square boundary residual method for the numerical solution of scattering problems," *IEEE Trans. Microwave Theory Tech.*, vol. MTT-21, pp. 99–104, Feb. 1973.

[5] W. Schlosser and H. G. Unger, "Partially filled waveguides and surface waveguides of rectangular cross section," *Adv. Microw.*, vol. 1, pp. 319–387, 1966.

[6] S. A. Schelkunoff, "Generalized telegraphist's equation for waveguides," *Bell Syst. Tech. J.*, vol. 31, pp. 784–801, 1952.

[7] C. C. Johnson, *Field and Wave Electrodynamics*. New York: McGraw-Hill, 1965.

[8] K. Ogusu, "Numerical analysis of the rectangular dielectric waveguide and its modifications," *IEEE Trans. Microwave Theory Tech.*, vol. MTT-25, pp. 874–885, Nov. 1977.

[9] F. E. Gardiol, "Higher order modes in dielectrically loaded rectangular waveguides," *IEEE Trans. Microwave Theory Tech.*, vol. MTT-16, pp. 919–924, Nov. 1968.

[10] A. S. Vander Vorst and R. J. M. Govaerts, "Application of a variation-iteration method to inhomogeneously loaded waveguides," *IEEE Trans. Microwave Theory Tech.*, vol. MTT-18, pp. 468–475, Aug. 1970.

[11] J. Askne, "An approach to linear and non-linear wave coupling using dispersion and energy relations," *Int. J. Electron.*, vol. 32, pp. 573–591, no. 5, 1972.

[12] P. R. McIsaac, "Symmetry-induced modal characteristic of uniform waveguides-I: Summary of results," *IEEE Trans. Microwave Theory Tech.*, vol. MTT-23, pp. 421–429, May 1976.

[13] J. Askne, S. Galt, and E. Kollberg, "A new design for 1-cm rutile traveling wave masers," to be published.

[14] T. C. L. G. Sollner, D. P. Clemens, T. L. Korzeniowski, G. C. McIntosh, E. L. Moore, and K. S. Yngvesson, "Low-noise 86-88-GHz traveling wave maser," *Appl. Phys. Lett.*, vol. 35 (11), pp. 833–835, Dec. 1979.

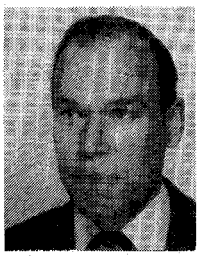

Jan I. H. Askne (S'63–M'65) was born in 1936. He received the Civilingenjör (M.Sc) degree in electrical engineering in 1961, and the Ph.D. degree in 1970 from Chalmers University of Technology, Göteborg, Sweden.

He has been University Lecturer since 1967 and has published articles on wave-propagation problems in complex media, radiation from molecules in cosmic clouds, and remote sensing problems. His present research interests are remote sensing of atmospheric water-vapor and temperature profiles and observation of cosmic molecular clouds.

Erik L. Kollberg was born in Stockholm, Sweden, in 1937. He received the Civilingenjör (M.Sc.) degree in electrical engineering in 1961 and the Ph.D. degree in 1970 from Chalmers University of Technology, Göteborg, Sweden.

Since 1961 he has been a member of the Research and Technical Staff of the Department of Electron Physics at Chalmers University of Technology and of the Onsala Space Observatory, Göteborg, Sweden. He was appointed Assistant Professor in 1971 and Professor in 1979. His research interest is primarily in the area of millimeter-wave mixers, masers, and receiver systems.

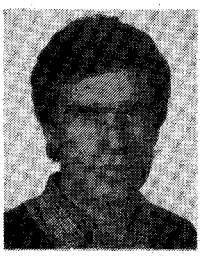

Lars Pettersson (M'74) was born on April 7, 1949. He received the Civ. Ing. and Ph. D. degrees in electrical engineering from Chalmers University of Technology, Göteborg, Sweden, in 1973 and 1979, respectively.

From 1973 to 1979 he was employed at the Electron Physics Department of Chalmers University of Technology as a Research Assistant working on maser slow-wave structures and microwave antennas. Since 1979 he has been employed at the Swedish National Defence Research Institute (FOA) in Linköping, Sweden, working on microwave scattering and antennas.